Stem Cell Research 18 (2017) 5–13

Contents lists available at ScienceDirect

Stem Cell Research

journal homepage: www.elsevier.com/locate/scr

The administration of multipotent stromal cells at precancerous stage precludes tumor growth and epithelial dedifferentiation of oral squamous cell carcinoma

Flavia Bruna *, Martha Arango-Rodríguez, Anita Plaza, Iris Espinoza, Paulette Conget

Centro de Medicina Regenerativa, Facultad de Medicina, Clínica Alemana Universidad del Desarrollo, Santiago, Chile

ARTICLE INFO

Article history:
Received 6 July 2016
Received in revised form 1 November 2016
Accepted 22 November 2016
Available online 1 December 2016

Keywords:
Multipotent stromal cells
Mesenchymal stem cells
Precancerous lesion
Oral squamous cell carcinoma
Papilloma

ABSTRACT

Multipotent stromal cells (MSCs) are envisioned as a powerful therapeutic tool. As they home into tumors, secrete trophic and vasculogenic factors, and suppress immune response their role in carcinogenesis is a matter of controversy. Worldwide oral squamous cell carcinoma (OSCC) is the fifth most common epithelial cancer.
Our aim was to determine whether MSC administration at precancerous stage modifies the natural progression of OSCC.
OSCC was induced in Syrian hamsters by topical application of DMBA in the buccal pouch. At papilloma stage, the vehicle or 3×10^6 allogenic bone marrow-derived MSCs were locally administered. Four weeks later, the lesions were studied according to: volume, stratification (histology), proliferation (Ki-67), apoptosis (Caspase 3 cleaved), vasculature (ASMA), inflammation (Leukocyte infiltrate), differentiation (CK1 and CK4) and gene expression profile (mRNA).
Tumors found in individuals that received MSCs were smaller than those presented in the vehicle group (87 ± 80 *versus* 54 ± 62 mm^3, $p < 0.05$). The rate of proliferation was two times lower and the apoptosis was 2.5 times higher in lesions treated with MSCs than in untreated ones. While the laters presented dedifferentiated cells, the former maintained differentiated cells (cytokeratin and gene expression profile similar to normal tissue).
Thus, MSC administration at papilloma stage precludes tumor growth and epithelial dedifferentiation of OSCC.

1. Introduction

Multipotent stromal cells, also referred to as mesenchymal stem cells (MSCs), are an heterogeneous subset of stromal cells present in several tissues including bone marrow, bone, adipose tissue, skin, kidney, umbilical cord and placenta (Friedenstein et al., 1968). The minimal criteria for defining MSCs are adherence to plastic surface; proliferation under the stimulus of fetal bovine serum; no expression of hematopoietic markers; expression of CD73, CD90, CD105, and differentiation into mesodermal cells (adipocytes, chondrocytes and osteocytes) (Dominici et al., 2006).

MSCs are envisioned as an ideal tool for cell therapy since they home into injured tissues whereas they could differentiate into tissue-specific cells (Ezquer et al., 2011), manage oxidative stress (Valle-Prieto and Conget, 2010), release trophic factors (Caplan and Dennis, 2006), promote neovascularization (Ball et al., 2007) or trigger an anti-inflammatory response (Uccelli and Prockop, 2010). It has been shown that donor MSCs also home into stablished tumors where they interact with cancer stem cells, regulate neovascularization and modulate the immune response (Al Moustafa et al., 2002; Bolontrade et al., 2012).

Currently, the role of MSCs in carcinogenesis is a matter of controversy. It has been reported that they favor tumor growth due to the immunosuppression (Djouad et al., 2003). Also, MSCs could enhance tumor metastatic potential since they can induce epithelia to mesenchyme transition (Huang et al., 2013). In contrast, it has been shown that MSCs inhibit tumorigenesis (Balasenthil et al., 2002a). The mechanisms apparently related to the antitumor effect could be: i) induction of cancer cell apoptosis (Ho et al., 2013), ii) avoidance of epithelium dedifferentiation (Ho et al., 2013), iii) inhibition of vascular network formation or apoptosis of vascular endothelial cells (Otsu et al., 2009; Secchiero et al., 2010), and iv) stimulation of anti-tumor immune response (Madrigal et al., 2014).

Worldwide oral squamous cell carcinoma (OSCC) is the fifth most common epithelial cancer, its annual incidence is over 300,000 diagnosed cases and its annual mortality is about 145,000 deaths (Rivera, 2015). Despite advances in its detection and treatment the mortality of OSCC remains high and its five-year survival rate is among the lowest of the major cancers (Rivera, 2015).

OSCC goes from normal keratinocyte transformation to random mutations linked to epigenetic processes that deregulate DNA repair

* Corresponding author at: Centro de Medicina Regenerativa, Facultad de Medicina Clínica Alemana-Universidad del Desarrollo, Av. Las Condes, 12,438, Santiago, Chile.
E-mail addresses: flabruna@gmail.com (F. Bruna), pconget@udd.cl (P. Conget).

http://dx.doi.org/10.1016/j.scr.2016.11.016

mechanisms, cell cycle, cell differentiation and apoptosis (Rivera, 2015). Thus, normal tissue evolves progressively through hyperplasia, dysplasia and carcinoma *in situ* until reaching the stage of invasive carcinoma (Rivera, 2015; Dvorak et al., 2011; Nishimura et al., 2012; Choi and Chen, 2005; Mendez et al., 2002; Arora et al., 2005).

The disease developed in the Syrian golden hamster using the mutagen 7.12-dimethylbenz-alpha-anthracene (DMBA) is a widely accepted animal model of OSCC (Chen et al., 2002; Nagini et al., 2009). It shares morphological, histological and molecular markers with human OSCC progression (Hasina et al., 2009; Ezquer et al., 2015; Aromando et al., 2014; Brandwein-Gensler et al., 2005).

The aim of this work was to determine whether MSC administration at precancerous stage modifies the natural progression of OSCC. For this, OSCC was induced in hamsters by topical application of DMBA in the buccal pouch. At papilloma stage, the vehicle or 3×10^6 allogenic bone marrow-derived MSCs were locally administered. Four weeks later, the lesions were studied according to their: volume (macroscopy), histology (H&E staining), rate of proliferation (immunohistofluorescence for Ki-67), rate of apoptosis (TUNEL), density of vasculature (immunohistofluorescence for ASMA), degree of inflammation (H&E and Toluidine blue staining), degree of differentiation (CK1 and CK4 immunohistofluorescence) and gene expression profile (RT-qPCR) (Supplementary Fig. 1).

2. Materials and methods

2.1. Animals

A total of 151 Syrian golden hamsters (*Mesocricetus auratus*) were used in this study. Nineteen were unmanipulated (5 used in OSCC natural progression study and 14 used in gene expression study), 56 served as MSC donors and 76 were OSCC induced (5 hyperplasia, 5 dysplasia, 5 papilloma and 5 carcinoma used in OSCC natural progression study; 14 OSCC + vehicle and 14 OSCC + MSC used for macroscopical and microscopical analysis, 14 OSCC + vehicle and 14 OSCC + MSC used for gene expression analysis).

Protocol was approved by the Ethic Committee of Facultad de Medicina Clinica Alemana-Universidad del Desarrollo (approval ID: 2011–14).

2.2. OSCC induction

Healthy male hamsters, eight weeks old, were painted thrice a week into their right buccal pouche with a N°4 camel-hair brush soaked with 50uL of mineral oil (Sigma-Aldrich, St. Louis, MO) or 50uL of 0.5% DMBA (Sigma-Aldrich) dissolved in mineral oil (Schwartz et al., 1988). Animals were housed at 22 °C, with a 12:12 h light-dark cycle, and water and food *ad libitum*.

2.3. Macroscopical analysis of OSCC progression

Nine and 13 weeks after the initiation of OSCC induction, hamsters were anesthetized by intraperitoneal injection of 20 mg/kg Xylazine (Centrovet, Santiago, Chile) and 20 mg/kg Ketamine (Ilium, Buenos Aires, Argentina). Buccal pouches were uncovered, and tumors were measured with a digital caliper (Mitutoyo Sul Americana LTDA, Brazil) and photographed using a digital camera (FUJIFILM-Finepi HS20 EXR). Two independent observers analyzed the photographs and described the lesions according to the presence of eritroplakia, leukoplakia, vascularization and exophytic or ulcerated rolled border nodules. The lesion volume was calculated using the formula: tumor volume (mm^3) = $0.52 \times [\text{width (mm)}]^2 \times \text{length (mm)}$ and the tumor increase was estimated as the ratio between final and initial volumes (Suzuki et al., 2011).

2.4. Microscopical analysis of OSCC progression

Four weeks after vehicle or MSC administration, hamsters were euthanized by an intraperitoneal injection of an overdose of Xylazine and Ketamine. Buccal pouches were procured and tumors were resected. Tumor specimens were fixed in 10% buffered formalin (Merck, USA), embedded in paraffin (Merck) and sectioned. Tissue sections of 4 μm were deparaffinized with Neoclear (Merck), rehydrated with graded alcohols, stained with H&E (Merck) and visualized with a light microscope (DM2000, Leica, Germany). Images were captured with a digital camera (DFC295, Leica). Tumor stage (hyperplasia, dysplasia, papilloma or carcinoma) was stated as previously described (Schwartz et al., 1988).

Histological analysis was performed in blind by three independent observers; one of them is a pathologist expert in oral diseases.

2.5. MSC isolation, ex vivo expansion and characterization

Healthy female hamsters, eight weeks old, were euthanized by an intraperitoneal injection of an overdose of Xylazine and Ketamine. Femurs and tibias were procured under sterile conditions. The epifisis were removed and bone marrow was collect by flushing bones with sterile phosphate buffer saline (PBS) (Gibco, Auckland, NZ). Recovered cells were resuspended in alpha-MEM (Gibco) supplemented with 10% fetal bovine serum (FBS, Gibco) and 40 mg/mL gentamycin (Sanderson Laboratory, Chile), and plated at a density of 0.25×10^6 nucleated cells/cm^2. Every three days, culture medium was changed. When foci reached confluence, adherent cells were detached with 0.25% trypsin, 2.65 mM EDTA (Gibco). After one subculture, cells were characterized and transplanted.

Immunophenotyping was performed by flow cytometry after immunostaining with APC-conjugated mouse anti-CD45 (BD Pharmingen, San Diego, USA), FITC-conjugated mouse anti-ASMA (Sigma), FITC-conjugated mouse anti-vimentin (Oncogen, USA) (Bartholomew et al., 2002). To assess the differentiation potential, cells were incubated with adipogenic or osteogenic differentiation media (Contador et al., 2015; Conget and Minguell, 1999). Seven and 14 days later, they were stained with Oil Red O or Alizarin Red, respectively.

2.6. MSC administration

When lesions reached the stage of papilloma, animals were randomly distributed to experimental groups, anesthetized and their buccal pouchs were exposed using a surgical forceps. Using a 23-gauge needle (Terumo, Tokio, Japón), 400 μL of 5% hamster plasma (vehicle) or 3×10^6 MSCs resuspended in 5% hamster plasma were injected into the mucosa around the lesions (Cavalieri and Rogan, 1992).

2.7. Proliferation assessment

Tissue sections of 5 μm were deparaffinized and rehydrated. After blocking with 5% FBS, samples were incubated overnight at 4 °C with a dilution 1:50 of rabbit anti-K-i67 polyclonal serum (Abcam, USA). Then, samples were washed and incubated 2 h at room temperature with a dilution 1:400 of Alexa488-conjugated goat anti-rabbit IgG (Cell Signaling, Massachusetts, USA). Cross-reactivity of the secondary antibody was tested incubating tissue sections without the primary antibody. Nuclei were counterstained with a dilution 1:1500 of DAPI (Invitrogen, California, USA). Samples were observed in a fluorescence microscope. Images were captured with a digital camera and analyzed using Image J software (NIH Image J). The rate of proliferation was calculated as the quotient between Ki-67-positive cells and the total number of cells, counted in five representative optical sections (at least 1000 nuclei) using 40× magnification (Hasina et al., 2009).

2.8. Apoptosis assessment

Tissue sections of 4 μm were deparaffinized, rehydrated, digested with 20 μg/mL proteinase K (Invitrogen) and labeled, following manufacturer instructions, with a terminal deoxynucleotidyl transferase dUTP nick 3′end-labeling (TUNEL) kit (Promega, USA). Nuclei were counterstained with a dilution 1:1500 of DAPI. Samples were observed in a fluorescence microscope. Images were captured with a digital camera and analyzed using Image J software. The rate of apoptosis was expressed as the number of TUNEL-positive cells per 1000 cells, observed in ten representative optical sections using 40× magnification. Areas with extensive necrosis were avoided (Ezquer et al., 2015).

2.9. Vascularization assessment

Tissue sections of 4 μm were deparaffinized, rehydrated, blocked with 5% FBS and incubated overnight at 4 °C with a dilution 1:50 of mouse anti-ASMA (Cell Marque, Rocklin, USA). Then, samples were washed and incubated two h at room temperature with a dilution 1:400 of Alexa488-conjugated goat anti-mouse IgG (Cell Signaling, USA). Cross-reactivity of the secondary antibody was tested incubating samples without the primary antibody. Nuclei were counterstained with a dilution 1:1500 of DAPI. Samples were observed in a fluorescence microscope, images were captured with a digital camera and analyzed using Image J software. The density of vasculature was expressed as the number of ASMA-positive vessels per field, observed in five representative optical sections using 40× magnification (Aromando et al., 2014).

2.10. Inflammation assessment

Tissue sections of 4 μm were deparaffinized, rehydrated and stained with H&E or with 1% Toluidine blue (Merck) in 1% sodium chloride solution (Sigma). Samples were visualized with a light microscope. Images were captured with a digital camera. The degree of inflammation was classified according to the score: absent (−), low (+), moderate (++) and severe (+++) (Brandwein-Gensler et al., 2005). The number of infiltrated mast cells was expressed as the number of metachromatic cells per field, observed in five representative optical sections using 40× magnification (Zaidi and Mallick, 2014).

2.11. Differentiation assessment

Tissue sections of 4 μm were deparaffinized, rehydrated, blocked with 5% FBS and incubated overnight at 4 °C with a dilution 1:50 of mouse anti-cytokeratin 1 (CK1, Abcam, Cambridge, UK) or mouse anti-cytokeratin 4 (CK4, Abcam). Then, samples were washed and incubated 2 h at room temperature with a dilution 1:400 of Alexa 488-conjugated goat anti-mouse IgG. Cross-reactivity of the secondary antibody was tested incubating samples without the primary antibody. Nuclei were counterstained with a dilution 1:1500 of DAPI. Samples were observed in a fluorescence microscope, images were captured with a digital camera and analyzed using Image J software. The expression of CK1 and CK4 was recorded as pixels intensity, in five representative optical sections using 40× magnification (Caster and Kahn, 2012).

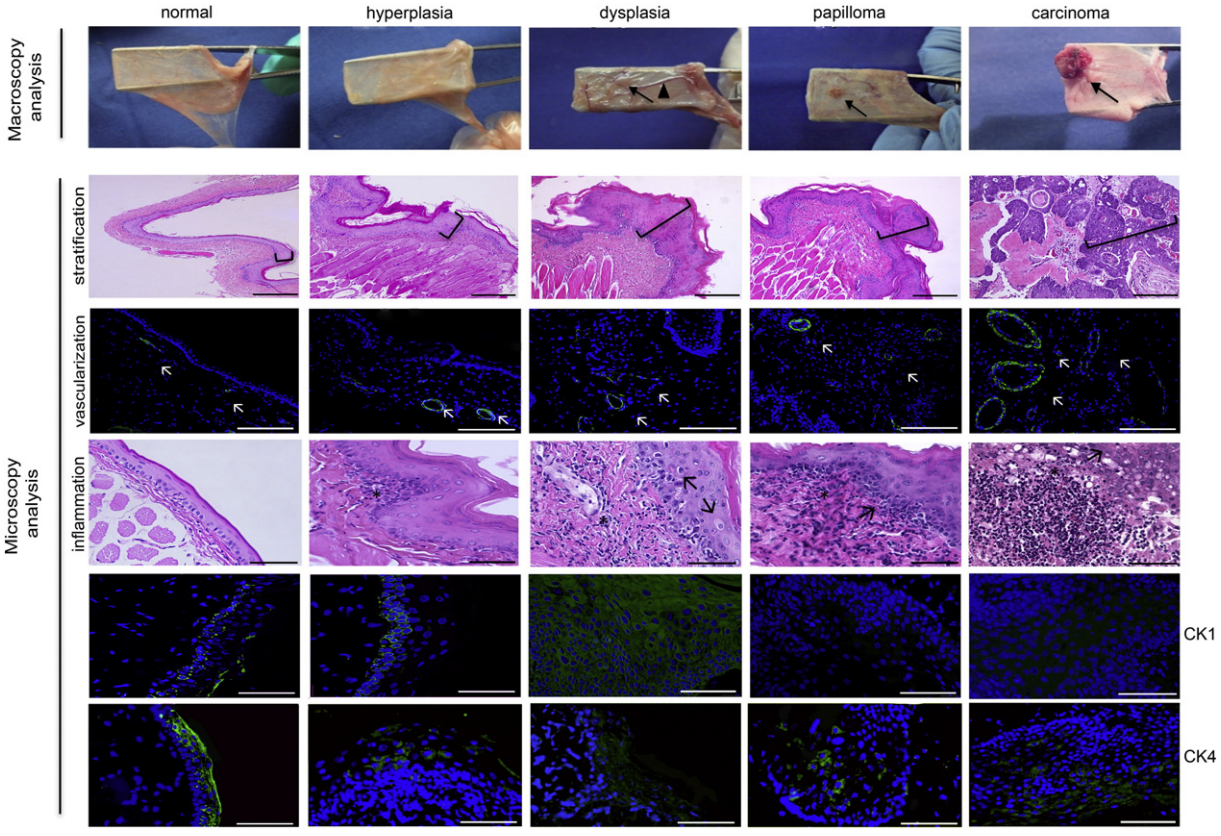

Fig. 1. OSCC progression. (First line) Macroscopy of buccal pouch. At dysplasia stage blood vessels were noticeable (arrow head). At papilloma stage, exophytic lesions appeared (black arrow). (Second line) Histology (H&E) of buccal pouch. The epithelium thickness changes over OSCC progression (square bracket). Bar = 100 μm. (Third line) Immunohistofluorescence for ASMA. The vascularization changes over OSCC progression (white arrow). Bar = 100 μm. (Fourth line) Histology (H&E) focusing in leukocyte infiltration (asterisk). Epithelial atypical cells were observed over OSCC progression (black arrow). Bar = 50 μm. (Fifth and Sixth lines) Immunohistofluorescence for CK1 and CK4, respectively. Bar = 50 μm. Representative images ($n = 5$).

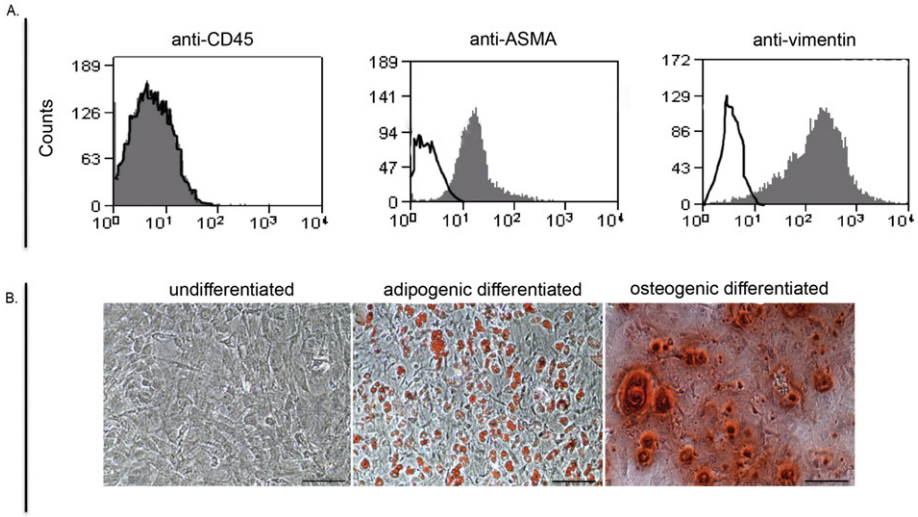

Fig. 2. Characterization of MSCs isolated from Syrian golden hamster bone marrow. (A) Immunophenotype of cells. White area = isotype control. (B) Differentiation assay. Bar = 100 μm. Representative data ($n = 4$).

2.12. Gene expression analysis

Total RNA was isolated from buccal pouches using RNEasy Plus Mini Kit (Qiagen, Hilden, Germany). Contaminating genomic DNA was degraded with DNAse RQ1 (Promega). One μg of RNA was reverse transcribed for 60 min at 42 °C using 200 U M-MLV reverse transcriptase (Invitrogen) and 0.5 μM oligo-dT primers (Invitrogen). Real time PCR was performed in a final volume of 10 μL containing 50 ng of cDNA,

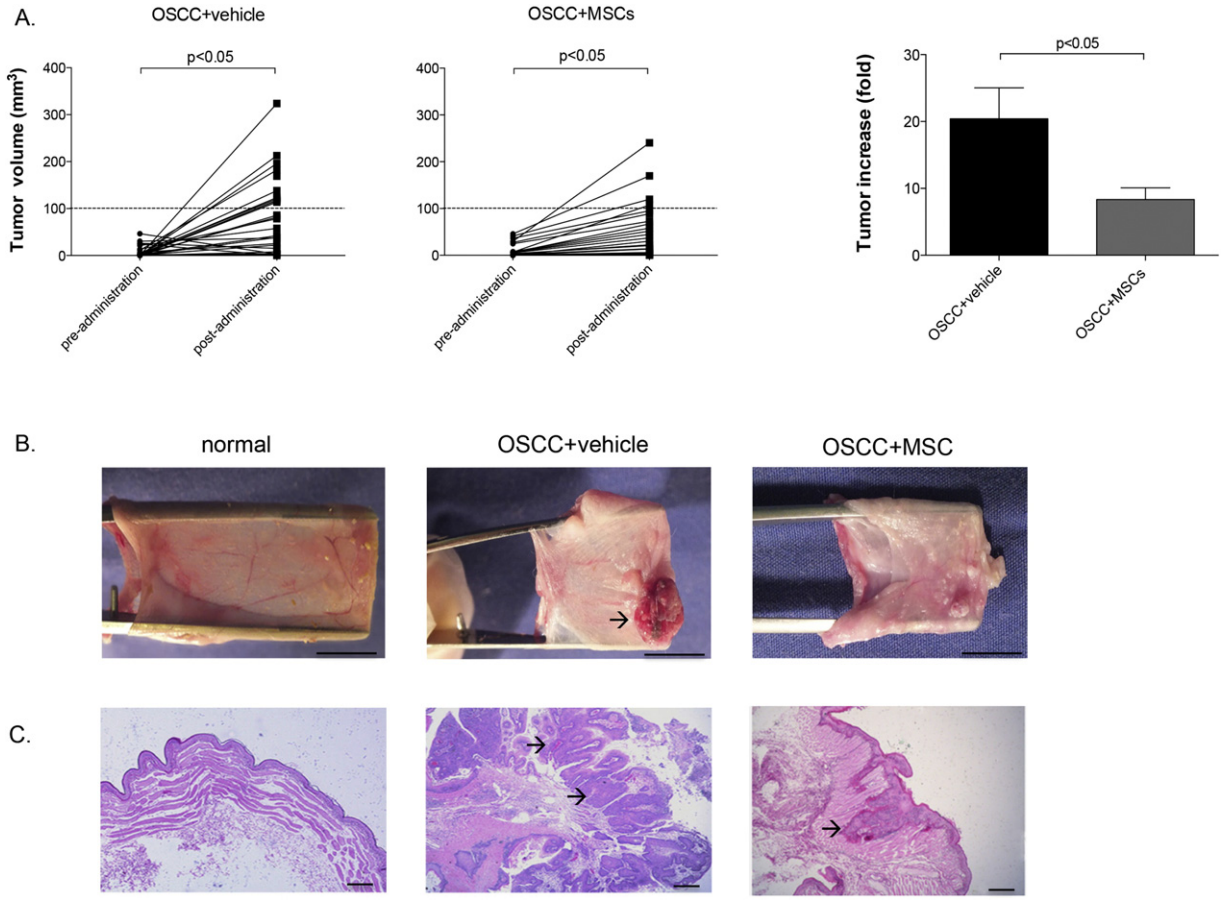

Fig. 3. MSC administration precludes OSCC tumor growth. (A) Tumor volume before (pre-) or four weeks after (post-) the administration of vehicle (OSCC + vehicle) or 3×10^6 cells (OSCC + MSCs). (B) Tumors increase four weeks after the administration of the vehicle (OSCC + vehicle) or 3×10^6 cells (OSCC + MSCs). (C) Macroscopy of buccal pouch four weeks after the administration of the vehicle (OSCC + vehicle) or 3×10^6 cells (OSCC + MSCs). Black arrow = necrosis features. Bar = 300 mm. (D) Histology (H&E) of buccal pouch. Black arrow = epithelium invasion. Bar = 100 μm. Representative data ($n = 14$).

Power SYBR Green PCR master mix (Life Technologies, Grand Island, NY) and 0.5 μM of each specific primer, using the Step One Plus PCR system (Life Technologies). Controls without reverse transcriptase were included. Amplicons were analyzed according to their size and melting temperature (Supplementary Table 1). To normalize data, 18S RNA was used as reference gene (Tobar et al., 2010). The mRNA level of a target gene was calculated using the 2ΔCt method and graphed as arbitrary units (a.u.) (Schmittgen and Livak, 2008).

2.13. Statistical analysis

As population distribution was non-parametric, comparison among groups were performed using one-way ANOVA test and Dunn's test as post-test. To compare between two groups, Tukey's test was used. StatGraph Prism 5.0 software was used for statistical analysis. Data are presented as median ± SEM. $p < 0.05$ was considered statistically significant.

3. Results

3.1. Natural progression of OSCC tumors

Buccal pouchs in normal hamsters were elastic and translucid (Fig. 1, first column). The epithelium was continuous and presented no more than four cell layers with scarce vasculature and absence of inflammation. CK1 was present in the epithelial basal cell layer and CK4 in the suprabasal cell layer.

The exposure to DMBA for four weeks resulted in hyperplasia (Fig. 1, second column). Buccal pouch retracted and showed leukoplakia and/or erythroplakia, accompanied by an engrossment of the mucosa due to inflammation. The epithelium showed 6–8 cell layers, no evidence of cell atypias or nuclear hypercromatism was found. Vessel size was increased and a few leukocyte foci were found. CK1 was present in the basal and suprabasal cell layers, and CK4 was increased in the suprabasal layer.

Dysplasia stage is evident after six weeks of exposure to DMBA (Fig. 1, third column). Buccal pouch engrossed and lose elasticity. The epithelium showed more than eight cell layers without invasion in to the stroma. An increase in vessel size and number, together with moderate leukocyte foci were observed. In addition, atypical cells were found. CK1 localized in the basal and CK4 in the suprabasal cell layers, both were over expressed.

At week 9 after first DMBA application papillomas appeared (Fig. 1, fourth column). Those exophytic lesions did not extend into the connective tissue but outgrowth from the surface. The histological analysis showed features of atypical cells in the epithelial layer but not invading the submucosal connective tissue. The number and size of vessels were increased in the stroma and epithelium compared with normal buccal pouch. Inflammation around the lesions was moderated. CK1 was undetectable and CK4 was increased and lose is suprabasal localization.

Carcinoma stage is reached after 13 weeks of exposure to DMBA (Fig. 1, fifth column). Buccal pouchs were contracted and stiffs, with features of necrosis. Epithelium showed abundant cell and nuclear pleomorphism, the stratification was lost and basal membrane was discontinuous. Aberrant vessels (large size and discontinuous wall) and inflammatory focus were abundant. CK1 disappeared and CK4 increased, being noticeable in all epithelial cell layers.

3.2. Phenotype of hamster MSCs

Adherent cells isolated from hamster bone marrow showed spindle-fibroblastic morphology and proliferate under the stimuli of FBS. They were negative for the hematopoietic marker CD45 and positive for the mesenchymal markers ASMA and vimentin (Fig. 2A). After exposure to the adipocyte differentiation medium, lipid drops stained with Oil Red O were observed (Fig. 2B). Exposure to the osteocyte differentiation

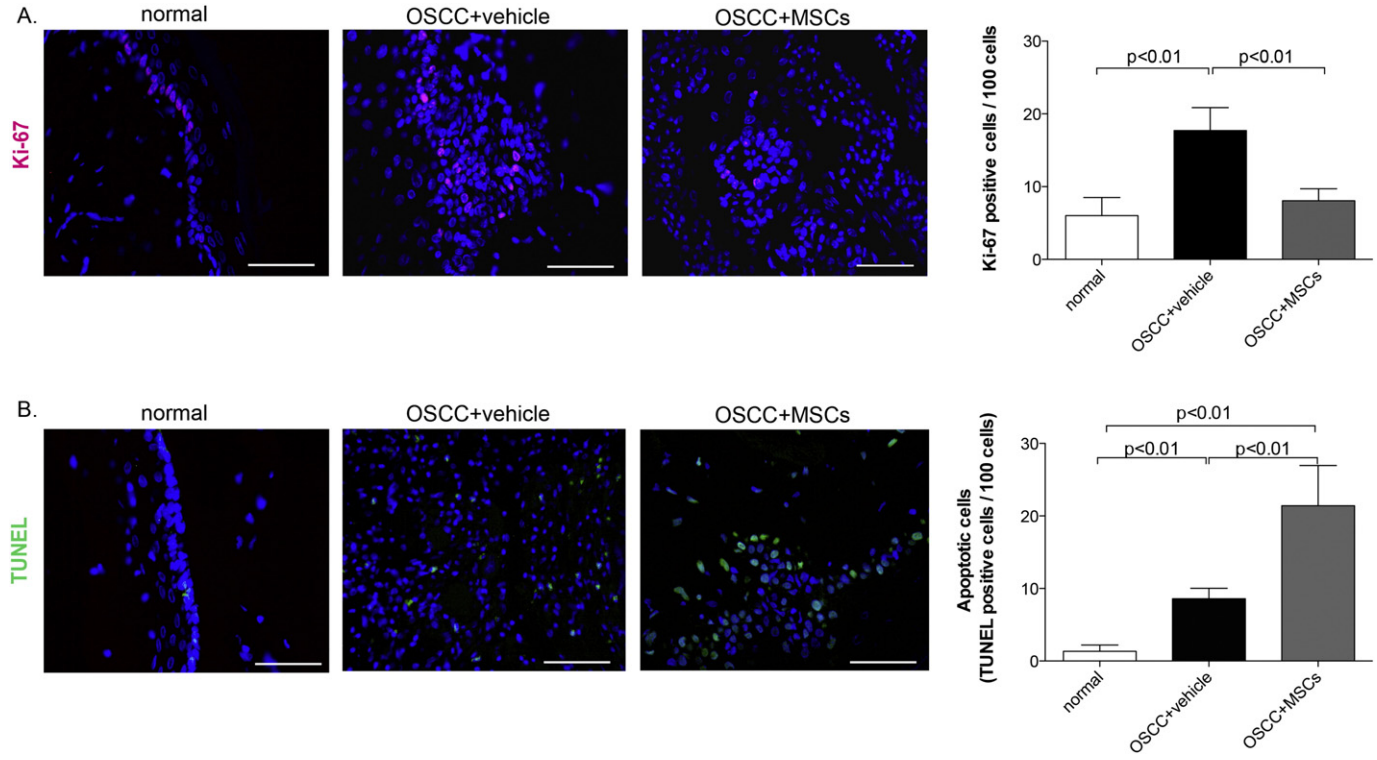

Fig. 4. MSC administration decreases proliferation and increases apoptosis in OSCC tumors. Four weeks after the administration of the vehicle (OSCC + vehicle) or 3×10^6 cells (OSCC + MSCs), (A) immunohistofluorescence for Ki-67 and (B) TUNEL assay. Bar = 50 μm. Representative images ($n = 8$).

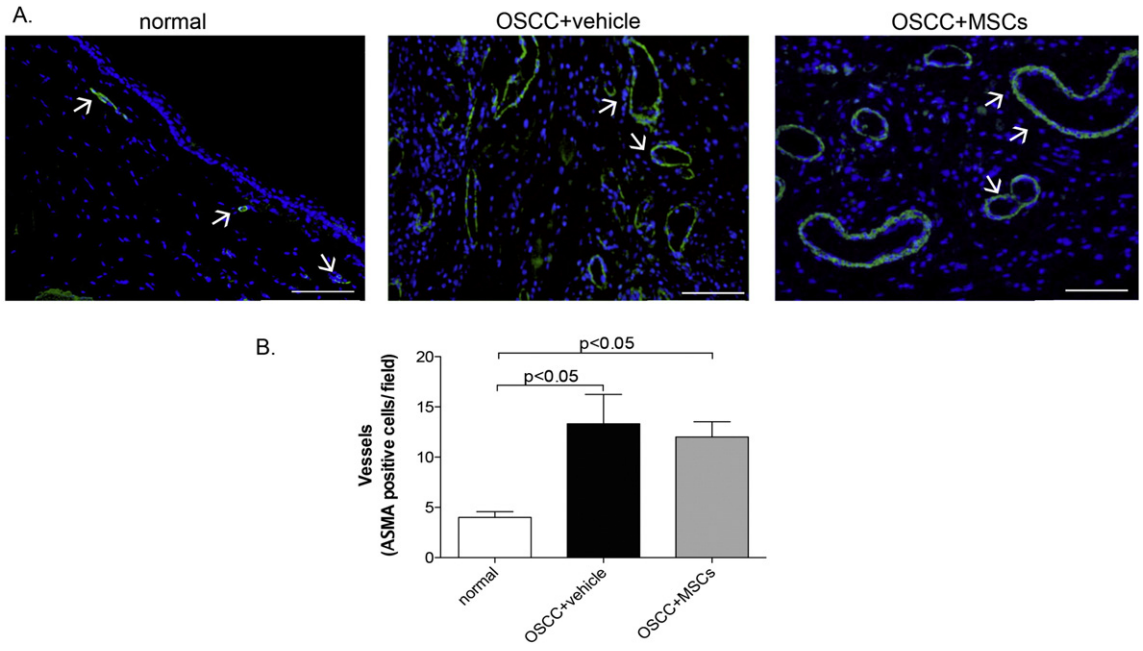

Fig. 5. MSC administration does not modify OSCC tumor vasculature density. Four weeks after the administration of the vehicle (OSCC + vehicle) or 3×10^6 cells (OSCC + MSCs), (A) immunohistofluorescence for ASMA. (B) Quantitative analysis. White arrow = vessel. Bar = 50 μm. Representative images ($n = 5$).

medium resulted in hydroxyapatite mineral depots that stained with Alizarin Red.

3.3. MSC administration precludes tumor growth and modifies the natural progression of OSCC tumors

Before MSC administration, 100% of the animals developed papilloma lesions which volume ranged from 1 to 50 mm^3. Four weeks later, all the hamsters presented tumors. Lesions receiving the vehicle grown up to 10 to 325 mm^3 and those receiving MSCs reached 5 to 220 mm^3 (Fig. 3A). Tumor volumes expressed as median ± SEM were 87 ± 80 and 54 ± 62 mm^3, respectively ($p < 0.05$). Together, tumor increase was three times lower in the later compared with the former ($p < 0.05$) (Fig. 3B). Population analysis showed that in the OSCC + vehicle group 90% of the animals presented tumors bigger than 100 mm^3, while in OSCC + MSCs group only 20% do so.

Tumors developed in animals that received the vehicle presented histological characteristics pathognomonic of carcinoma stage including necrosis features, poorly differentiated epithelial cells, disorganized basal cell layer and cell invasion into the stroma (Fig. 3C). In constrast, in the animals transplanted with MSCs the tumors presented no necrosis, well-differentiated epithelial cells and continuous basal layer.

3.4. MSC administration decreases the rate of proliferation and increases the rate of apoptosis in OSCC tumors

The rate of proliferation was significantly lower in the tumors of hamsters that received MSCs compared with those that received the vehicle (18 ± 7 *versus* 8 ± 4 Ki-67-positive cells/100 cells, $p < 0.05$) (Fig. 4A). Conversely, the rate of apoptosis was significantly higher in the former compared with the later (9 ± 4 *versus* 21 ± 16 TUNEL-positive cells/100 cells, $p < 0.05$) (Fig. 4B).

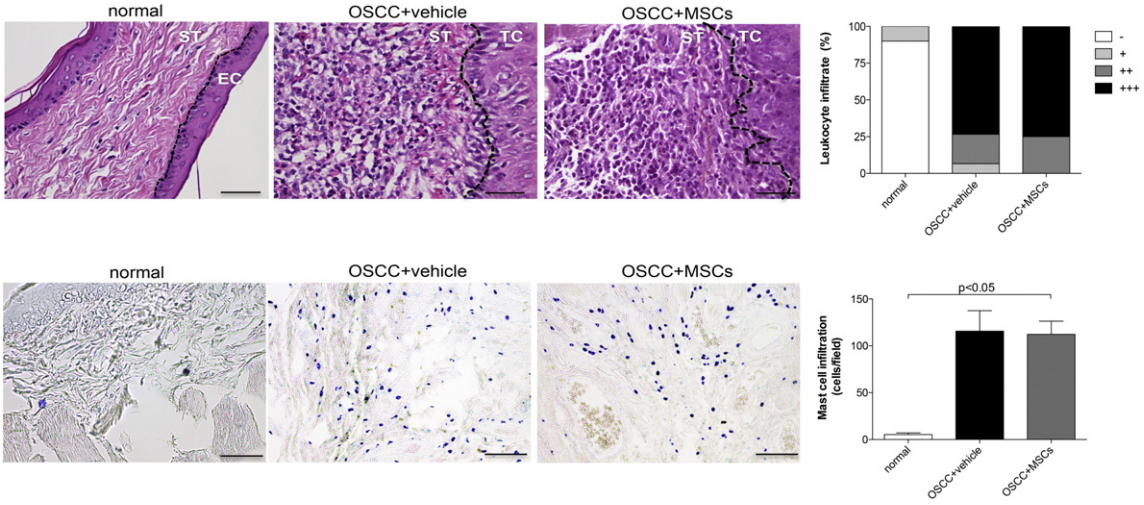

Fig. 6. MSC administration does not modify OSCC tumor inflammation. Four weeks after the administration of the vehicle (OSCC + vehicle) or 3×10^6 cells (OSCC + MSCs), (A) histology (H&E) focusing in leukocyte infiltration. EC = epithelial cells, ST = stroma, TC = tumor cells. Graphs show quantitative analysis of leukocyte infiltrate according to the following score: *absent* (−), *low* (+), *moderate* (++) and *severe* (+++). (B) Toluidine blue staining. Graphs show quantitative analysis of mast cells abundance. Bar = 50 μm. Representative images ($n = 5$).

3.5. MSC administration modified neither the density of vasculature nor the degree of inflammation in OSCC tumors

Irrespective of MSC administration, tumors presented large blood vessels with wall discontinuity (Fig. 5A). Their abundance was higher than observed in normal tissue (Fig. 5B).

MSC administration did not modify tumor inflammation evaluated as either leucocyte or mast cell infiltration (Fig. 6).

3.6. MSC administration prevents epithelial dedifferentiation in OSCC tumors

In papilloma lesions treated with MSCs it was possible to detect CK1 (Fig. 7A). On another hand, CK4 expression was restricted to the epithelium cell layer and epithelial cells invading the stroma (nest sheets) and its total level was lower in lesions receiving MSCs compared to those receiving the vehicle (Fig. 7A).

Quantitative analysis of mRNA levels of ECGR2 (proliferation related gene), BTC (survival related gene), TRIM2 (migration related gene) and EAF2 (transcriptional activity related gene) showed that, compared with untreated OSCC, these genes were significantly down-regulated in the lesions treated with MSCs, reaching normal values (Fig. 7B).

4. Discussion

The effect of donor MSCs in tumor growth remains controversial (Cho et al., 2009). Discrepancies concerned to whether they promote or suppress it may be due to disparities in cell source, isolation and expansion conditions, *via* and timing of administration, cancer model, timing of assessment, *etc.* (Ikebe and Suzuki, 2014). Up to our knowledge, the impact of donor MSCs in precancerous lesions has not been reported. We decided to test it in the OSCC model settled in Syrian golden hamster because it mimics the etiology (DMBA is present in cigarette smoke), the progression and the response to chemopreventive agents of human OSCC (Nagini et al., 2009). Together, changes are grossly visible and patognomonic of each stage (Nagini et al., 2009). When we administered 0.1×10^6 or 1×10^6 MSCs to OSCC lesions at papilloma stage we observed a reduction in tumor size (Supplementary Fig. 2). This effect was more significant when we administered 3×10^6 MSCs (Fig. 3).

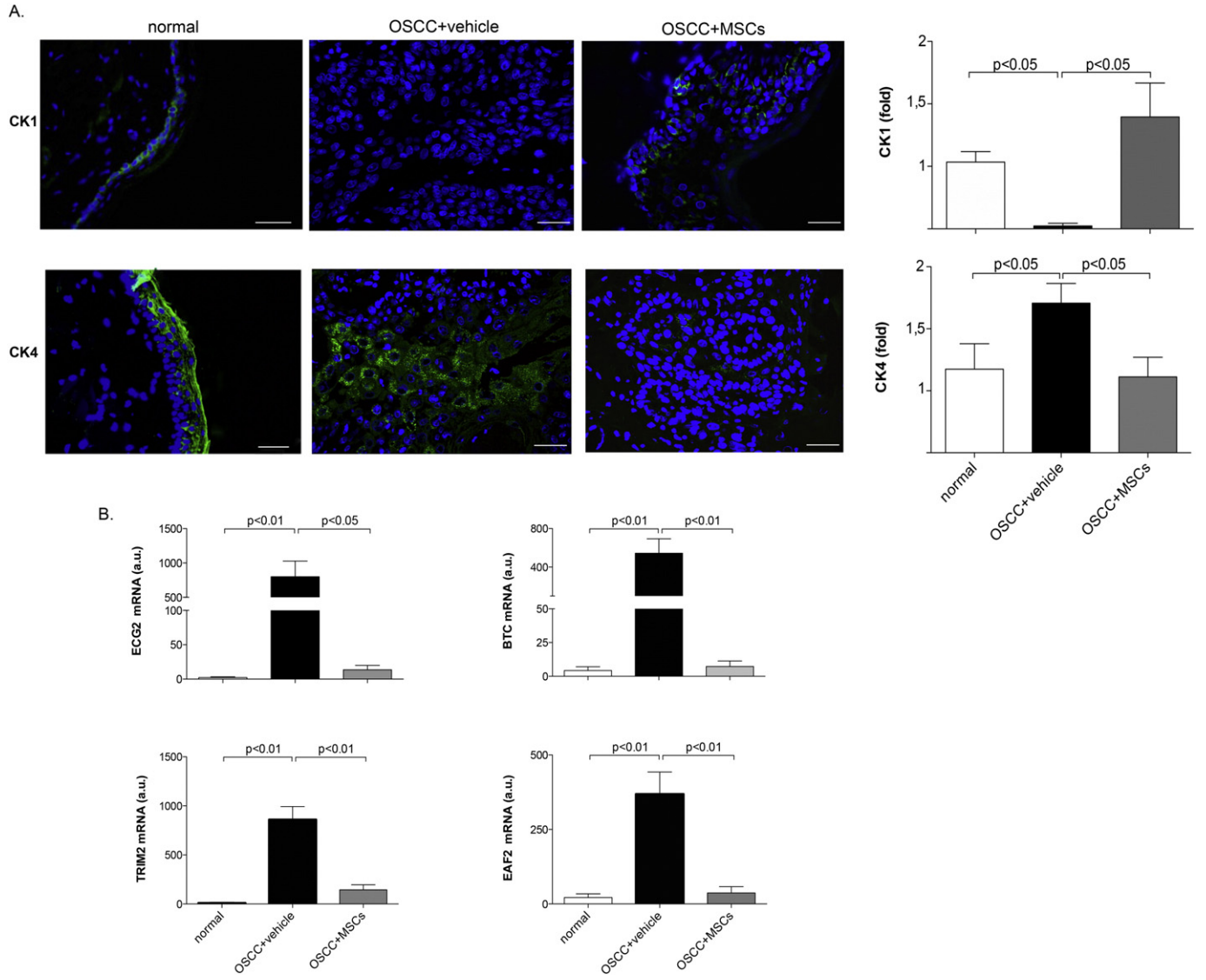

Fig. 7. MSC administration precludes OSCC tumor epithelial dedifferentiation. Four weeks after the administration of the vehicle (OSCC + vehicle) or 3×10^6 cells (OSCC + MSCs), (A) immunohistofluorescence for CK1 and CK4. Graphs show quantitative analysis. White bar = 50 μm. ($n = 5$). (C) Gene expression of ECG2, BTC, Trim2 and Eaf2. Representative images ($n = 14$).

The observed anti-tumorigenic effect of MSCs correlates with a decrease in cell proliferation and an increase in cell apoptosis. Both constrain tumor size enlargement. These results are consistent with previous works reporting that MSC administration inhibits established tumor growth through proliferation inhibition and apoptosis induction (Ramasamy et al., 2007; Qiao et al., 2008; Glennie et al., 2005; Beyth et al., 2005).

Neovascularization plays a central role in the development and progression of tumors including OSCC (Li et al., 2007). It has been previously shown that MSCs differentiate and secrete vasculogenic growth factors supporting tumor vasculature (Roorda et al., 2009). In a glioma animal model it has been shown that the systemic administration of MSCs reduced the number and caliber of tumor vessels (Ho et al., 2013). Thus, depending on yet undefined variables MSCs can promote or inhibit neovascularization. Under the setting here presented, donor MSCs does not modify the vasculature of OSCC lesions (Fig. 5).

Since neoplastic microenvironment is similar to that of an injured tissue. Man (2010) donor MSCs delivered around OSCC papilloma could trigger a non-specific allogeneic immune response that might impedes tumor growth. At the end of the study period we observed no differences in the infiltration of leukocyte or mast cells (first host line defense in the oral mucosa (Coussens et al., 1999)). Thus, chronic immunomodulation does not explain MSC anti-tumorigenic effect. We cannot rule out that acute immunomodulation is involved.

Cytokeratins are epithelial specific intermediate filament proteins, underlying distinct cellular properties and differentiation stages (Schweizer et al., 2006). In the hamster buccal pouch, the epithelial basal cell layer expresses CK1 while the suprabasal cell layer express CK4 (Balasenthil et al., 2002a; Balasenthil et al., 2002b). Alterations in CK1 and CK4 expression are sensitive markers for epithelial tumor stratification (Ogden et al., 1996). Thus, the observed recovery of CK1 expression and the normalization of CK4 tissue distribution after MSC administration reflect an avoidance of epithelium dedifferentiation. Accordingly, it has been reported that MSCs stabilize cell phenotype of keratinocytes, endothelial cells, pericytes and monocytes in wound repair (Sasaki et al., 2008). Further support to the preclusion of dedifferentiation is the normalization of gene expression profile after MSC administration (Fig. 7B). The later has been observed in other oral pathological conditions (Dowdall et al., 2015). The preservation of a differentiated phenotype may be attributed to the potential of MSCs to sustain a homeostatic microenvironment, particularly scavenging oxidative stress (Valle-Prieto and Conget, 2010; Ramasamy et al., 2007).

Taken together, our results support an anti-tumorigenic effect of MSCs in epithelial precancerous lesions. Thus, the local administration of allogeneic MSCs should be envisioned as a preventive strategy for the development of OSCC since donor cells modify its natural progression and improve prognosis due to the preservation of epithelial phenotype. This is not an irrelevant goal in the field since the prognosis for patients with OSCC still poor (Jadhav and Gupta, 2013).

5. Conclusion

The local administration of allogenic bone marrow-derived MSCs, at papilloma stage, precludes tumor growth and epithelial dedifferentiation of OSCC.

Supplementary data to this article can be found online at http://dx.doi.org/10.1016/j.scr.2016.11.016.

Conflict of interest

Authors declare no conflict of interest.

Acknowledgements

This work was supported by FONDECYT grant # 1130760 (P.C.).

References

Al Moustafa, A.E., Alaoui-Jamali, M.A., Batist, G., Hernandez-Perez, M., Serruya, C., Alpert, L., Black, M.J., Sladek, R., Foulkes, W.D., 2002. Identification of genes associated with head and neck carcinogenesis by cDNA microarray comparison between matched primary normal epithelial and squamous carcinoma cells. Oncogene 21, 2634–2640.

Aromando, R.F., Raimondi, A.R., Pérez, M.A., Trivillin, V.A., Schwint, A.E., Itoiz, M.E., 2014. Angiogenesis in potentially malignant lesions and carcinomas during experimental oral carcinogenesis. Anticancer Res. 34, 6381–6388.

Arora, S., Matta, A., Shukla, N.K., Deo, S.V., Ralhan, R., 2005. Identification of differentially expressed genes in oral squamous cell carcinoma. Mol. Carcinog. 42, 97–108.

Balasenthil, S., Rao, K.S., Nagini, S., 2002a. Altered cytokeratin expression during chemoprevention of experimental hamster buccal pouch carcinogenesis by garlic. J. Oral Pathol. Med. 31, 142–146.

Balasenthil, S., Rao, K.S., Nagini, S., 2002b. Altered cytokeratin expression during chemoprevention of experimental hamster buccal pouch carcinogenesis by garlic. J. Oral Pathol. Med. 31, 142–146.

Ball, S.G., Shuttleworth, C.A., Kielty, C.M., 2007. Mesenchymal stem cells and neovascularization: role of platelet-derived growth factor receptors. J. Cell. Mol. Med. 11, 1012–1030.

Bartholomew, A., Sturgeon, C., Siatskas, M., Ferrer, K., McIntosh, K., Patil, S., Hardy, W., Devine, S., Ucker, D., Deans, R., Moseley, A., Hoffman, R., 2002. Mesenchymal stem cells suppress lymphocyte proliferation in vitro and prolong skin graft survival in vivo. Exp. Hematol. 30, 42–48.

Beyth, S., Borovsky, Z., Mevorach, D., Liebergall, M., Gazit, Z., Aslan, H., Galun, E., Rachmilewitz, J., 2005. Human mesenchymal stem cells alter antigen-presenting cell maturation and induce T-cell unresponsiveness. Blood 105, 2214–2219.

Bolontrade, M.F., Sganga, L., Piaggio, E., Viale, D.L., Sorrentino, M.A., Robinson, A., Sevlever, G., Garcia, M.G., Mazzolini, G., Podhajcer, O.L., 2012. A specific subpopulation of mesenchymal stromal cell carriers overrides melanoma resistance to an oncolytic adenovirus. Stem Cells Dev. 21, 2689–2702.

Brandwein-Gensler, M., Teixeira, M.S., Lewis, C.M., Lee, B., Rolnitzky, L., Hille, J.J., Genden, E., Urken, M.L., Wang, B.Y., 2005. Oral squamous cell carcinoma: histologic risk assessment, but not margin status, is strongly predictive of local disease-free and overall survival. Am. J. Surg. Pathol. 29, 167–178.

Caplan, A.I., Dennis, J.E., 2006. Mesenchymal stem cells as trophic mediators. J. Cell. Biochem. 98, 1076–1084.

Caster, A.H., Kahn, R.A., 2012. Computational method for calculating fluorescence intensities within three-dimensional structures in cells. Cell Logist. 2, 176–188.

Cavalieri, E.L., Rogan, E.G., 1992. The approach to understanding aromatic hydrocarbon carcinogenesis. The central role of radical cations in metabolic activation. Pharmacol. Ther. 55, 183–199.

Chen, Y.K., Hsue, S.S., Lin, L.M., 2002. The mRNA expression of inducible nitric oxide synthase in DMBA-induced hamster buccal-pouch carcinomas using reverse transcription-polymerase chain reaction. J. Oral Pathol. Med. 31, 82–86.

Cho, J.A., Park, H., Kim, H.K., Lim, E.H., Seo, S.W., Choi, J.S., Lee, K.W., 2009. Hyperthermia-treated mesenchymal stem cells exert antitumor effects on human carcinoma cell line. Cancer 115, 311–323.

Choi, P., Chen, C., 2005. Genetic expression profiles and biologic pathway alterations in head and neck squamous cell carcinoma. Cancer 104, 1113–1128.

Conget, P.A., Minguell, J.J., 1999. Phenotypical and functional properties of human bone marrow mesenchymal progenitor cells. J. Cell. Physiol. 181, 67–73.

Contador, D., Ezquer, F., Espinosa, M., Arango-Rodriguez, M., Puebla, C., Sobrevia, L., Conget, P., 2015. Dexamethasone and rosiglitazone are sufficient and necessary for producing functional adipocytes from mesenchymal stem cells. Exp. Biol. Med. 9, 1235–1246.

Coussens, L., Raymond, W., Bergers, G., Laig-Webster, M., Behrendtsen, O., Werb, Z., Caughey, H., Hanahan, D., 1999. Inflammatory mast cells up-regulate angiogenesis in OSCC. Genes Dev. 11, 1382–1397.

Djouad, F., Plence, P., Bony, C., Tropel, P., Apparailly, F., Sany, J., Noël, D., Jorgensen, C., 2003. Immunosuppressive effect of mesenchymal stem cells favors tumor growth in allogeneic animals. Blood 102, 3837–3844.

Dominici, M., Le Blanc, K., Mueller, I., Slaper-Cortenbach, I., Marini, F., Krause, D., Deans, R., Keating, A., Prockop, D., Horwitz, E., 2006. Minimal criteria for defining multipotent mesenchymal stromal cells. The International Society for Cellular Therapy position statement. Cytotherapy 8, 315–317.

Dowdall, J.R., Sadow, P.M., Hartnick, C., Vinarsky, V., Mou, H., Zhao, R., Song, P.C., Franco, R.A., Rajagopal, J., 2015. Identification of distinct layers within the stratified squamous epithelium of the adult human true vocal fold. Laryngoscope 125, E313–E319.

Dvorak, H.F., Weaver, V.M., Tlsty, T.D., Bergers, G., 2011. Tumor microenvironment and progression. J. Surg. Oncol. 103, 468–474.

Ezquer, M., Ezquer, F., Ricca, M., Allers, C., Conget, P., 2011. Intravenous administration of multipotent stromal cells prevents the onset of non-alcoholic steatohepatitis in obese mice with metabolic syndrome. J. Hepatol. 55, 1112–1120.

Ezquer, F., Giraud-Billoud, M., Carpio, D., Cabezas, F., Conget, P., Ezquer, M., 2015. Proregenerative microenvironment triggered by donor mesenchymal stem cells preserves renal function and structure in mice with severe diabetes mellitus. Biomed. Res. Int. 20, 164–703.

Friedenstein, A., Petrakova, K., Kurolesova, A., Frolova, G., 1968. Heterotopic transplants of bone marrow. Transplantation 6, 230–247.

Glennie, S., Soeiro, I., Dyson, P.J., Lam, E.W., Dazzi, F., 2005. Bone marrow mesenchymal stem cells induce division arrest anergy of activated T cells. Blood 105, 2821–2827.

Hasina, R., Martin, L.E., Kasza, K., Jones, C.L., Jalil, A., Lingen, M.W., 2009. ABT-510 is an effective chemopreventive agent in the mouse 4-nitroquinoline 1-oxide model of oral carcinogenesis. Cancer Prev. Res. 2, 385–393.

Ho, I.A., Toh, H.C., Ng, W.H., Teo, Y.L., Guo, C.M., Hui, K.M., Lam, P.Y., 2013. Human bone marrow-derived mesenchymal stem cells suppress human glioma growth through inhibition of angiogenesis. Stem Cells 31, 146–155.

Huang, W.H., Chang, M.C., Tsai, K.S., Hung, M.C., Chen, H.L., Hung, S.C., 2013. Mesenchymal stem cells promote growth and angiogenesis of tumors in mice. Oncogene 32, 4343–4354.

Ikebe, C., Suzuki, K., 2014. Mesenchymal stem cells for regenerative therapy: optimization of cell preparation protocols. Biomed. Res. Int. 2014, 1–11.

Jadhav, K.B., Gupta, N., 2013. Clinicopathological prognostic implicators of oral squamous cell carcinoma: need to understand and revise. N. Am. J. Med. Sci. 5 (12), 671–679 (*PMC*).

Li, C., Chen, J.C., Wang, Z.H., Zhang, B., Li, B., Song, Y.F., 2007. The characteristics and significance of microvessel in oral squamous cell carcinoma. Chin. J. Stomatol. 42, 70–73.

Madrigal, M., Rao, K.S., Riordan, N.H., 2014. A review of therapeutic effects of mesenchymal stem cell secretions and induction of secretory modification by different culture methods. J. Transl. Med. 12, 260.

Man, Y., 2010. Aberrant leukocyte infiltration: a direct trigger for breast tumor invasion and metastasis. Int. J. Biol. Sci. 6, 129–132.

Mendez, E., Cheng, C., Farwell, D.G., Ricks, S., Agoff, S.N., Futran, N.D., Weymuller Jr., E.A., Maronian, N.C., Zhao, L.P., Chen, C., 2002. Transcriptional expression profiles of oral squamous cell carcinomas. Cancer 95, 1482–1494.

Nagini, S., Letchoumy, P.V., T.A., R. Cr, 2009. Of humans and hamsters: a comparative evaluation of carcinogen activation, DNA damage, cell proliferation, apoptosis, invasion, and angiogenesis in oral cancer patients and hamster buccal pouch carcinomas. Oral Oncol. 45, 31–37.

Nishimura, K., Semba, S., Aoyagi, K., Sasaki, H., Yokozaki, H., 2012. Mesenchymal stem cells provide an advantageous tumor microenvironment for the restoration of cancer stem cells. Pathobiology J. Immun. Mol. Cell. Biol. 79, 290–306.

Ogden, G.R., Chisholm, D.M., Lane, E.B., 1996. The utility of cytokeratin profiles for detecting oral cancer using exfoliative cytology. Br. J. Oral Maxillofac. Surg. 34, 461–466.

Otsu, K., Das, S., Houser, S.D., Quadri, S.K., Bhattacharya, S., Bhattacharya, J., 2009. Concentration-dependent inhibition of angiogenesis by mesenchymal stem cells. Blood 113, 4197–4205.

Qiao, L., Xu, Z.L., Zhao, T.J., Ye, L.H., Zhang, X.D., 2008. Dkk-1 secreted by mesenchymal stem cells inhibits growth of breast cancer cells via depression of Wnt signalling. Cancer Lett. 269, 67–77.

Ramasamy, R., Lam, E.W., Soeiro, I., Tisato, V., Bonnet, D., Dazzi, F., 2007. Mesenchymal stem cells inhibit proliferation and apoptosis of tumor cells: impact on in vivo tumor growth. Leukemia 21, 304–310.

Rivera, C., 2015. Essential of oral cancer. Int. J. Clin. Exp. Pathol. 8, 11884–11894.

Roorda, B.D., ter Elst, A., Kamps, W.A., de Bont, E.S., 2009. Bone marrow-derived cells and tumor growth: contribution of bone marrow-derived cells to tumor micro-environments with special focus on mesenchymal stem cells. Crit. Rev. Oncol. Hematol. 69, 187–198.

Sasaki, M., Abe, R., Fujita, Y., Ando, S., Inokuma, D., Shimizu, H., 2008. Mesenchymal stem cells are recruited into wounded skin and contribute to wound repair by transdifferentiation into multiple skin cell type. J. Immunol. 180, 2581–2587.

Schmittgen, T.D., Livak, K.J., 2008. Analyzing real-time PCR data by the comparative CT method. Nat. Protoc. 3, 1101–1108.

Schwartz, J., Shklar, G., Reid, S., Trickler, D., 1988. Prevention of experimental oral cancer by extracts of Spirulina-Dunaliella algae. Nutr. Cancer 11, 127–134.

Schweizer, J., Bowden, P.E., Coulombe, P.A., Langbein, L., Lane, E.B., Magin, T.M., Maltais, L., Omary, M.B., Parry, D.A., Rogers, M.A., Wright, M.W., 2006. New consensus nomenclature for mammalian keratins. J. Cell Biol. 174, 169–174.

Secchiero, P., Zorzet, S., Tripodo, C., Corallini, F., Melloni, E., Caruso, L., Bosco, R., Ingrao, S., Zavan, B., Zauli, G., 2010. Human bone marrow mesenchymal stem cells display anticancer activity in SCID mice bearing disseminated non-Hodgkin's lymphoma xenografts. PLoS One 5, e11140.

Suzuki, K., Sun, R., Origuchi, M., Kanehira, M., Takahata, T., Itoh, J., Umezawa, A., Kijima, H., Fukuda, S., Saijo, Y., 2011. Mesenchymal stromal cells promote tumor growth through the enhancement of neovascularization. Mol. Med. 17, 579–587.

Tobar, N., Guerrero, J., Smith, P.C., Martinez, J., 2010. NOX4-dependent ROS production by stromal mammary cells modulates epithelial MCF-7 cell migration. Br. J. Cancer 103, 1040–1047.

Uccelli, A., Prockop, D.J., 2010. Why should mesenchymal stem cells (MSCs) cure autoimmune diseases? Curr. Opin. Immunol. 22, 768–774.

Valle-Prieto, A., Conget, P.A., 2010. Human mesenchymal stem cells efficiently manage oxidative stress. Stem Cells Dev. 19, 1885–1893.

Zaidi, M., Mallick, A., 2014. A study on assessment of mast cells in oral squamous cell carcinoma. Ann. Med. Health Sci. Res. 4, 457–460.